

# Positively Charged Polyprodrug Amphiphiles with Enhanced Drug Loading and Reactive Oxygen Species-Responsive Release Ability for Traceable Synergistic Therapy

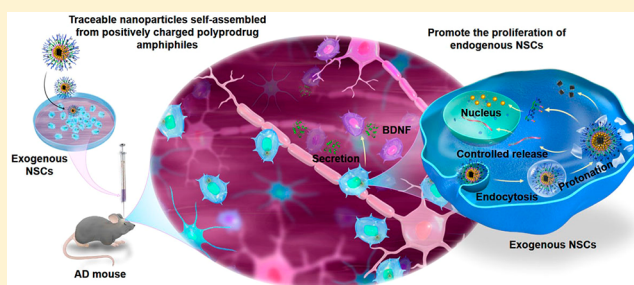
Yan Li,<sup>†</sup> Yanhui Li,<sup>†</sup> Weihong Ji,<sup>†,‡</sup> Zhiguo Lu,<sup>†,‡</sup> Linying Liu,<sup>†,‡</sup> Yuanjie Shi,<sup>†</sup> Guanghui Ma,<sup>†</sup> and Xin Zhang<sup>\*,†</sup>

<sup>†</sup>State Key Laboratory of Biochemical Engineering, Institute of Process Engineering, Chinese Academy of Sciences, Beijing 100190, China

<sup>‡</sup>University of Chinese Academy of Sciences, Beijing 100049, China

## Supporting Information

**ABSTRACT:** Due to the vast differences in chemical properties among small molecule drugs, nucleotide drugs, and superparamagnetic iron oxide nanocubes (SPIONs), such as charge and hydrophobicity, entrapment of these within a single carrier for traceable synergistic therapy has been proven difficult. Herein, we synthesize positively charged polyprodrug amphiphiles. The hydrophobic polyprodrug unit of the amphiphiles is positively charged, which can simultaneously load hydrophobic SPIONs and absorb negative let-7b antisense oligonucleotide to construct traceable co-delivery nanoparticles (NPs). This characteristic avoids the use of inert materials and enhances drug loading of the traceable NPs. The traceable NPs can achieve controlled release of drugs to reduce the differentiation of exogenous neural stem cells (NSCs) and enhance their secretion of brain-derived neurotrophic factor (BDNF) synergistically. Exogenous NSCs treated with the NPs significantly rescue the memory deficits in 2xTg-AD mice. In addition, the transplantation site and migration of exogenous NSCs can be traced using the SPIONs with high  $r_2$  value for magnetic resonance imaging. Therefore, traceable NPs self-assembled from the positively charged polyprodrug amphiphiles may have the potential to open up a new avenue for treatment of Alzheimer's disease (AD), as well as other neurodegenerative disorders.



## INTRODUCTION

Alzheimer's disease (AD) is the most common neurodegenerative disease characterized by neuronal loss and causes cognitive and memory deterioration and further impairs daily activities.<sup>1</sup> Multiple lines of evidence suggest that neurogenesis by endogenous neural stem cells (NSCs) and survival of newly differentiated cells can contribute to self-repair after neuronal loss.<sup>2</sup> However, endogenous NSCs cannot fully compensate for the neuronal loss due to their limited number. Although injection of brain-derived neurotrophic factor (BDNF) has been explored for promoting the proliferation of NSCs, its short half-life in blood and limited targeting ability reduce the potential therapeutic efficacy.<sup>3</sup> Therefore, it is crucial to find a method to enhance the level of BDNF in the diseased site for AD therapy.

An attractive approach is the transplantation of exogenous NSCs, which can express BDNF.<sup>4</sup> Importantly, an unexpected and potentially valuable characteristic of NSCs has recently been revealed that they are highly migratory and seem to be attracted to the area of brain pathology.<sup>5</sup> Therefore, implantation of exogenous NSCs can elevate the level of BDNF in the diseased site to activate the proliferation of

endogenous NSCs for the treatment of AD. However, there are two disadvantages limiting the efficiency of exogenous NSCs: (i) Under normal conditions, the amount of BDNF in NSCs is very low, and it dramatically decreases during NSC differentiation.<sup>6</sup> (ii) It is difficult to trace NSCs in real time after transplantation, which is problematic because the therapeutic efficacy depends on their transplantation site and subsequent migration.<sup>7</sup> Therefore, improved application of exogenous NSCs should reduce differentiation, upregulate the BDNF level and permit long-term tracing in real time.

To satisfy these conditions, here we propose a strategy for utilizing traceable synergistic therapy to control exogenous NSCs as BDNF source for AD therapy. The lethal-7 (let-7) gene is the first known human micro-RNA (miRNA) that is expressed in the brain NSCs. The overexpression of let-7b leads to decreased proliferation and promotes differentiation of NSCs by targeting the stem cell regulator TLX (NR2E1). The use of antisense RNA oligonucleotide against let-7b (let-7b antisense oligonucleotide) can down-regulate the level of let-7b

Received: February 9, 2018

Published: February 27, 2018

and upregulate the TLX expression, which reduce the differentiation of NSCs.<sup>8</sup> Hydrophobic simvastatin is shown to elevate the expression of BDNF in the hippocampus and enhance the recovery of spatial learning.<sup>9</sup> Therefore, we suggest to combine these two drugs, let-7b antisense oligonucleotide and simvastatin, to reduce the differentiation of exogenous NSCs and enhance their secretion of BDNF synergistically. This will significantly improve the therapeutic efficacy for AD. To allow traceability, superparamagnetic iron oxide nanocubes (SPIONs) can trace exogenous NSCs due to their high  $r_2$  relaxivity in magnetic resonance imaging (MRI).<sup>10</sup> Unfortunately, this method cannot be directly implemented due to the intrinsic deficiencies of these two drugs and SPIONs, including poor stability and membrane permeability, that reduce both therapeutic efficacy and traceability.<sup>11</sup> Hence, it is urgent to conquer the deficiencies of these two drugs and SPIONs simultaneously.

A common strategy is to utilize co-delivery nanoparticles (NPs) that would ensure each NSC receives both drugs and SPIONs without having to time sequential doses.<sup>12</sup> However, due to the vast differences in chemical properties between drugs and SPIONs, such as charge and hydrophobicity, entrapment of these within a single carrier has been proven difficult. Although NPs self-assembled from triblock polymers are always used for coencapsulation, there are several barriers hindering their application.<sup>13</sup> First, these polymers with inert materials are the major component while drugs are the minor.<sup>14</sup> For brain disease, a high dose of these excipients may cause systemic toxicity and accentuate further disease.<sup>15</sup> Second, intracellular trafficking of polymeric carriers has identified endosomal/lysosomal release to be the rate-limiting step because the contents are generally routed for lysosomal degradation.<sup>16</sup> Third, simple encapsulation of hydrophobic drugs typically causes premature burst release in the physiological environment, which seriously reduces the bioavailability of drugs.<sup>17</sup> Therefore, how best to exploit the use of polymers to increase drug loading and achieve controlled release of drugs in the active site is an important direction of study to facilitate effective clinical transformation.

Herein, we intended to develop positively charged polyprodrug amphiphiles to meet these conditions. Our group reported previously that hydrophilic zwitterionic poly-(carboxybetaine) (PCB) could maintain the stability of NPs and accelerate endosomal/lysosomal escape via protonation.<sup>18</sup> Inspired by the unique structure of PCB, we proposed to conjugate simvastatin to part of the carboxylate group of PCB to form the polyprodrug amphiphiles PCB-Se–Se-simvastatin (PCB-Se–Se-Sim) (Figure 1). The reactive oxygen species (ROS)-labile diselenide bond (-Se–Se-) was used as a linker because NSCs maintain a high ROS status, which provides an enabling environment for simvastatin to be selectively released in NSCs.<sup>19</sup> Different from the neutral polyprodrug unit in amphiphiles reported previously,<sup>20</sup> the hydrophobic polyprodrug unit of PCB-Se–Se-Sim was positively charged, which could simultaneously load hydrophobic SPIONs and absorb negative let-7b antisense oligonucleotide to construct traceable PCB-Se–Se-Sim/SPIONs/let-7b antisense oligonucleotide NPs (CSeM/let-7b NPs) (Scheme 1a). This characteristic avoided the use of inert materials and enhanced the drug loading of the traceable co-delivery NPs.

The mechanism that the traceable CSeM/let-7b NPs controlled exogenous NSCs as BDNF source for AD therapy was shown in Scheme 1b. The traceable CSeM/let-7b NPs

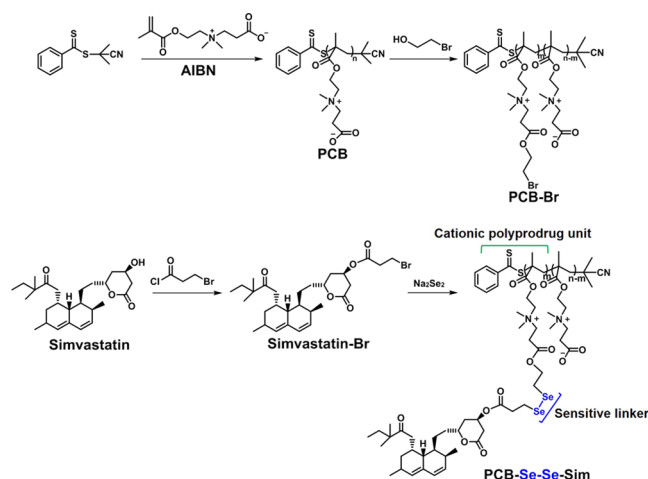
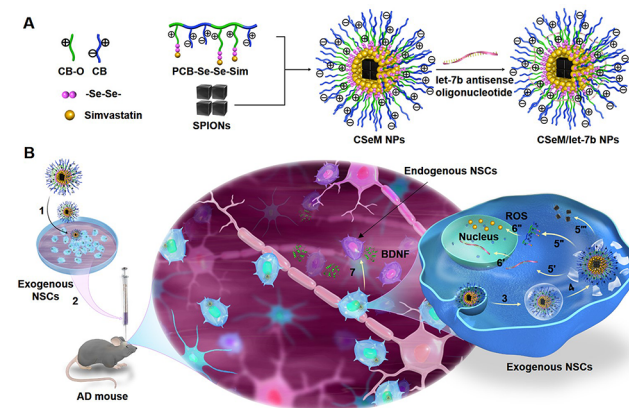


**Figure 1.** Synthetic routes of the polyprodrug amphiphiles PCB-Se–Se-Sim.

### Scheme 1. Illustration of Strategy for Construction and Functionalization of the Traceable CSeM/let-7b NPs<sup>a</sup>



<sup>a</sup>(A) Preparation of the traceable CSeM/let-7b NPs. Polyprodrug amphiphiles were self-assembled to load SPIONs and absorb let-7b antisense oligonucleotide. (B) Schematic illustration of the mechanism of the traceable CSeM/let-7b NPs controlling exogenous NSCs as BDNF source for AD therapy. After being added into culture medium (1), exogenous NSCs with CSeM/let-7b NPs were transplanted into AD mice (2). NPs would be internalized into endosomes/lysosomes (3), in which PCB was protonated (4) to accelerate the release of the let-7b antisense oligonucleotide (5'), PCB-Se–Se-Sim polymer (5'') and SPIONs (5''') into cytoplasm. The let-7b antisense oligonucleotide (6') and simvastatin released via the breakage of diselenide bond (6'') entered the nuclei to enhance the secretion of BDNF, which could promote the proliferation of endogenous NSCs for AD therapy (7). During this process, the transplantation site and migration of exogenous NSCs were traced in real time by SPIONs for MRI.

could be added to the culture medium (1) and exogenous NSCs with NPs were then transplanted into the brain of AD mice by stereotactic injection (2). CSeM/let-7b NPs would be internalized into endosomes/lysosomes (3), in which the carboxylate group of PCB was protonated (4) to accelerate the release of the let-7b antisense oligonucleotide (5'), PCB-Se–Se-Sim polymer (5'') and SPIONs (5''') into cytoplasm. The let-7b antisense oligonucleotide could then decrease the differentiation of exogenous NSCs (6'). Simvastatin was released via the breakage of the diselenide bond induced by ROS and entered the nuclei to enhance the secretion of BDNF

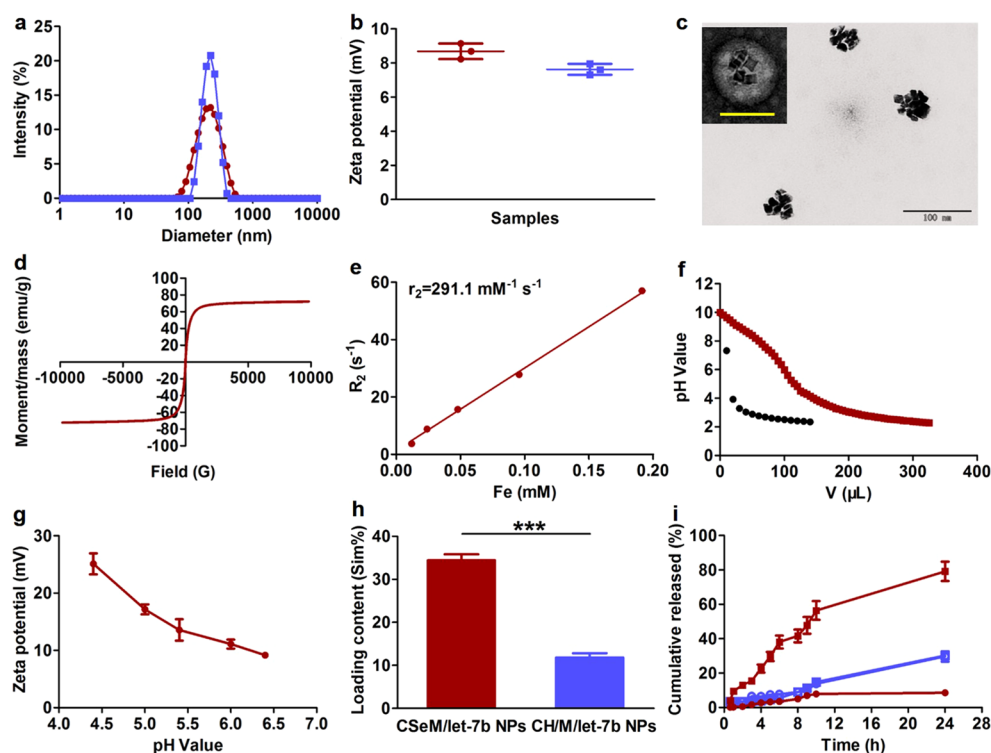


**Figure 2.** Characterization of the traceable NPs. (a) The diameter and (b) zeta potential of NPs at the N/P ratio of 5 detected by dynamic light scattering: (●) CSeM/let-7b NPs; (■) CH/M/let-7b NPs. (c) TEM image of CSeM/let-7b NPs. The inset image is TEM image with negative staining. The scale bar of inset image = 100 nm. (d) The magnetization curve of CSeM/let-7b NPs. (e) The  $r_2$  value of CSeM/let-7b NPs. (f) The buffering capacity of CSeM/let-7b NPs. The buffering capacity was detected by acid–base titration in 0.01 M NaCl aqueous solution: (●) NaCl aqueous solution. (■) CSeM/let-7b NPs solution. (g) The zeta potential of CSeM/let-7b NPs at different pH values detected by dynamic light scattering. (h) The simvastatin loading content detected using UV–vis spectroscopy with a characteristic absorbance peak at 278 nm. (i) The cumulative release of simvastatin at 37 °C in 0.5% Tween-80 PBS or 0.5% Tween-80 PBS with 0.01% H<sub>2</sub>O<sub>2</sub>. (red circles) CSeM/let-7b NPs in 0.5% Tween-80 PBS; (red squares) CSeM/let-7b NPs in 0.5% Tween-80 PBS with 0.01% H<sub>2</sub>O<sub>2</sub>; (blue circles) CH/M/let-7b NPs in 0.5% Tween-80 PBS; (blue squares) CH/M/let-7b NPs in 0.5% Tween-80 PBS with 0.01% H<sub>2</sub>O<sub>2</sub>. Free simvastatin was detected using HPLC. The mean  $\pm$  SD is shown ( $n = 3$ ). \*\*\* $P < 0.005$ .

(6<sup>''</sup>). The BDNF could promote the proliferation of endogenous NSCs for AD therapy (7). During this process, the transplantation site and migration of exogenous NSCs were traced in real time by SPIONs for MRI. Therefore, the traceable NPs self-assembled from the positively charged polyprodrug amphiphiles could control exogenous NSCs as BDNF source for traceable synergistic therapy of AD.

## RESULTS AND DISCUSSION

PCB polymer with molecular weight of 11.65 kDa was synthesized via reversible addition–fragmentation chain transfer polymerization (RAFT) (Figure 1 and Figure S1a). The diselenide bond-containing polyprodrug amphiphile PCB-Se–Se-Sim with molecular weight of 35.99 kDa was then synthesized through the reaction of disodium diselenide (Na<sub>2</sub>Se<sub>2</sub>) (Figure S1b).<sup>21</sup> The structures of intermediates and end products were detected by <sup>1</sup>H NMR, which indicated the successful synthesis (Figure S2). The selenium (Se) element in the polymer was confirmed by inductively coupled plasma mass spectrometry (ICP-MS) with a characteristic absorbance peak at 196.025 nm and the concentration of Se element was 141.7  $\mu$ g/mg (Figure S3). Calculated from these results of gel permeation chromatography (GPC) and ICP-MS, approximate 60% of PCB were successfully linked with simvastatin via diselenide bond. PCB-hexanol (PCB-H) amphiphiles with the same conjugation efficiency of inert material 1-hexanol were

successfully synthesized to construct traceable PCB-H/simvastatin/SPIONs/let-7b antisense oligonucleotide NPs (CH/M/let-7b NPs) (Figure S4). For comparison, simvastatin was physically encapsulated in the CH/M/let-7b NPs.

The polyprodrug amphiphile PCB-Se–Se-Sim was a random copolymer, in which CB-Se–Se-Sim was hydrophobic and CB was hydrophilic. The random copolymer could self-assemble into stable NPs in aqueous solution in which the hydrophobic CB-Se–Se-Sim was the core and the hydrophilic CB was the corona.<sup>22</sup> The self-assembling ability of both amphiphiles was detected by the critical micelle concentration (CMC). The CMC was reached when the fluorescence intensity of Nile red exhibited an abrupt variation with the increasing concentration of amphiphiles. PCB-Se–Se-Sim polyprodrug amphiphiles had a lower CMC of 40  $\mu$ g/mL (Figure S5), indicating that amphiphiles with hydrophobic simvastatin polyprodrug exhibited a stronger self-assembling ability.

Next, CSeM/let-7b NPs were prepared to study their effect on exogenous NSCs. Hydrophobic cubic SPIONs of about 20 nm in diameter were synthesized via high temperature thermal decomposition (Figure S6). CSeM and CH/M NPs had a comparable diameter of approximate 150 nm with zeta potential values of 15.30 and 15.77 mV, respectively (Figure S7). Both NPs could completely absorb the let-7b antisense oligonucleotide at an N/P ratio of 5, as demonstrated by gel electrophoresis (Figure S8). These results indicated that the

cationic polyprodrug unit could efficiently absorb the negative let-7b antisense oligonucleotide. At the N/P ratio of 5, the diameter of the CSeM/let-7b NPs was 199.8 nm (Figure 2a) with a zeta potential of 8.69 mV (Figure 2b). It was 243.5 nm for the CH/M/let-7b NPs with a zeta potential of 7.63 mV (Figure S9). Because excess materials might impose an increased burden for patients to excrete, NPs with N/P ratio of 5 were selected and utilized for the following experiments.

The morphology of the final NPs was characterized using a transmission electron microscope (TEM). The TEM images demonstrated that SPIONs were aggregated in the CSeM/let-7b NPs and CH/M/let-7b NPs after encapsulation (Figure 2c and Figure S10). The loading efficiency and content of SPIONs in the assembled NPs were detected using ICP-MS. The loading efficiency of SPIONs for both NPs was comparable, and it was 72.60% for CSeM/let-7b NPs and 56.11% for CH/M/let-7b NPs (Figure S11a). The loading content showed the same trend that it was 12.67% for CSeM/let-7b NPs and 10.06% for CH/M/let-7b NPs (Figure S11b). The magnetization curve exhibited no remnant magnetization and coercivity (Figure 2d and Figure S12). These results demonstrated that SPIONs are superparamagnetic at room temperature before and after encapsulation. Furthermore, the magnetic property of CSeM/let-7b NPs was monitored by the  $r_2$  value calculated by measuring the change in the spin–spin relaxation rate ( $R_2$ ) per unit iron concentration. The traceable CSeM/let-7b NPs had an  $r_2$  value of  $291.1 \text{ mM}^{-1} \text{ s}^{-1}$  (Figure 2e), which was sufficiently high for in vivo MRI application.

The acidic endosomes/lysosomes were the rate-limiting step of NPs in cells as drugs needed to escape from the endosomes/lysosomes and reach the cytosol to exert their therapeutic effect.<sup>23</sup> In the polyprodrug amphiphiles, the hydrophilic unit was PCB, which could accelerate the endosomal/lysosomal escape of NPs via protonation. The buffering capacity of the traceable NPs was investigated by acid–base titration in 0.01 M NaCl aqueous solution. The result demonstrated that PCB modification had a good buffering capacity over the pH range of 7.4 to 3.5 (Figure 2f). The zeta potential of CSeM/let-7b NPs showed a pH dependency, whereby the zeta potential increased from 9.17 at pH 6.4 to 25.1 at pH 4.4 (Figure 2g). The pH buffering capacity of PCB might be benefit for the endosomal/lysosomal escape of the traceable NPs by proton sponge effect in acidic endosomes (pH 5.0–6.0) and lysosomes (pH 4.5–5.0).<sup>24</sup>

The loading content of simvastatin was detected using UV–vis spectroscopy with a characteristic absorbance peak at 278 nm. It was 34.41% for the CSeM/let-7b NPs, significantly higher than that of CH/M/let-7b NPs (11.81%) due to their minor inert materials (Figure 2h). Next, the ROS-responsiveness of NPs was tracked using high performance liquid chromatography (HPLC) (Figure S13). Simvastatin was released via the breakage of diselenide bond induced by  $\text{H}_2\text{O}_2$ . The diselenide bond can be easily oxidized to selenenic acid.<sup>25</sup> Free simvastatin was released after treatment with esterase, which is abundant in cytoplasm. As shown in Figure 2i, 29.69% simvastatin was released for the physically loaded CH/M/let-7b NPs in phosphate buffered saline (PBS, pH = 7.4) due to premature burst release and  $\text{H}_2\text{O}_2$  had almost no effect on their release rate. CSeM/let-7b NPs released 8.55% simvastatin after 24 h incubation in PBS, indicating that they were stable in a physiological environment. The presence of  $\text{H}_2\text{O}_2$  accelerated the release rate, with 79.13% released after incubation in 0.01%  $\text{H}_2\text{O}_2$  for 24 h. As anticipated, the presence

of  $\text{H}_2\text{O}_2$  accelerated the release rate of simvastatin via the breakage of the diselenide bond, which was abundant in the cytoplasm of NSCs.<sup>19</sup>

To investigate the effect of the traceable NPs on exogenous NSCs, cells were isolated from the hippocampus of sucking mice. Nestin is a widely employed marker of multipotent NSCs.<sup>26</sup> The isolated cells were nestin-positive, indicating that they were NSCs and suitable for the following experiments (Figure S14). Emerging evidence now suggested that proliferative, self-renewing multipotent NSCs maintained a high ROS status.<sup>27</sup> Our results demonstrated that the isolated NSCs were ROS-positive, which would benefit for the controlled release of simvastatin (Figure S15). Before in vivo application, the biocompatibility of the traceable NPs on exogenous NSCs was studied using a 3-(4,5-dimethylthiazol-2-yl)-2,5-diphenyltetrazolium bromide (MTT) assay. With the increased concentration of amphiphiles, the cell viability was decreased (Figure S16a). It was 85.1% at the concentration of  $6.25 \mu\text{g/mL}$  and decreased to 47.4% at the concentration of  $50.0 \mu\text{g/mL}$  for CSeM NPs. After the NPs were complexed with let-7b antisense oligonucleotide, the cell viability was increased due to the lower positive charge of the complexes. The cell viability was approximately 100% at an N/P ratio of 5 for NPs with let-7b antisense oligonucleotide, rendering these NPs suitable for in vivo application (Figure S16b).

Next, the internalization of NPs was analyzed by flow cytometry using a carboxyfluorescein (FAM)-labeled let-7b antisense oligonucleotide (FAM-let-7b) as a fluorescent probe. The mean fluorescence intensity of FAM for both NPs in NSCs was comparable, where CSeM/FAM-let-7b and CH/M/FAM-let-7b NPs exhibited about 157.1 and 136.3 times the intensity of free FAM-let-7b, respectively. These results suggested that NPs could significantly enhance the cellular uptake of the let-7b antisense oligonucleotide (Figure 3a,b).

The intracellular trafficking of CSeM/let-7b NPs was further investigated using a confocal laser scanning microscope (CLSM). The green fluorescence of FAM-let-7b was initially associated with endosomes/lysosomes stained by LysoTracker Red as yellow dots with an overlap coefficient of 0.77 after 2 h incubation (Figure 3c,d). At 4 h, most signal corresponding to the FAM-let-7b did not overlap with the endosomes/lysosomes, indicating efficient endosomal/lysosomal escape due to the protonation of PCB.<sup>28</sup> The CH/let-7b NPs without loading simvastatin had the same trend in endosomal/lysosomal escape, indicating that the loading of simvastatin on the NPs had almost no effect on the process of endosomal/lysosomal escape (Figure S17). Furthermore, the single-stranded oligonucleotides in cytoplasm could rapidly accumulate in nuclei that some fluorescence of the FAM-let-7b antisense oligonucleotide was overlapped with nuclei stained with 4',6-diamidino-2-phenylindole (DAPI) as arrows shown (Figure 3e).<sup>29</sup> To confirm whether the protonation of PCB was benefit for the endosomal/lysosomal escape of the NPs, the endosomal/lysosomal escape of NPs was detected in the presence of bafilomycin A1. Bafilomycin A1 is a proton pump inhibitor, which selectively inhibits the vacuolar  $\text{H}^+$ -ATPase and prevents the acidification of endosomes/lysosomes, and is used to study the proton sponge effect (Figure 3f).<sup>30</sup> Compared with the NSCs without treatment with bafilomycin A1 (Figure 3g(i)), bafilomycin A1 obviously inhibited the endosomal/lysosomal escape of FAM-let-7b antisense oligonucleotide such that almost no fluorescence of FAM-let-7b antisense oligonucleotide was overlapped with nuclei (Figure 3g(ii)).

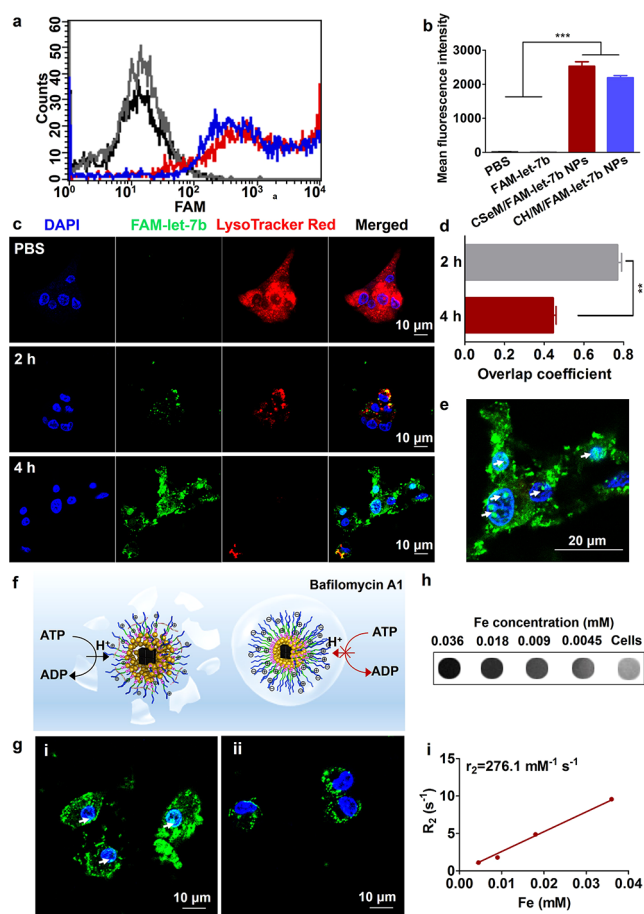


**Figure 3.** Cellular uptake and endosomal/lysosomal escape of the traceable NPs. (a) Cellular uptake of NPs after incubation for 4 h detected by flow cytometry. (b) Mean fluorescence intensity quantified from Figure 3a. (c) Assessment by CLSM of endosomal/lysosomal escape after 2 and 4 h of incubation. (d) Overlap coefficient of FAM-let-7b and LysoTracker Red was quantified from panel c using software in CLSM. (e) Magnified image of panel c at 4 h. The FAM-let-7b antisense oligonucleotide was overlapped with the nuclei stained with DAPI as arrows shown. Endosomes/lysosomes were stained with LysoTracker Red. (f) The mechanism of bafilomycin A1 that inhibited vacuolar  $H^+$ -ATPase and prevented the acidification of endosomes/lysosomes. (g) Assessment by CLSM of the distribution of FAM-let-7b antisense oligonucleotide in NSCs after culture with CSeM/FAM-let-7b NPs for 4 h. The NSCs were treated without (i) or with (ii) bafilomycin A1 (bafilomycin A1, 200 nM for 30 min before the transfection and continued during the transfection). The nuclei were stained with DAPI. (h) MR phantom of NSCs after internalization of CSeM/let-7b NPs for 4 h. Samples showed concentration-dependent contrasts. Darker contrast indicated stronger  $T_2$  relaxation enhancement for each concentration. (i) The  $r_2$  value of the NSCs after internalization of CSeM/let-7b NPs for 4 h. All MRI studies were conducted on a 7 T MRI scanner. The mean  $\pm$  SD is shown ( $n = 3$ ). \*\* $P < 0.01$ , \*\*\* $P < 0.005$ .

These results indicated that the protonation of PCB in acidic endosomes/lysosomes could promote the endosomal/lysosomal escape of FAM-let-7b antisense oligonucleotide via proton sponge effect.

The MR sensitivity of the labeled NSCs after uptake of the CSeM/let-7b NPs was detected using a 7 T MRI scanner. An MR phantom study confirmed that high  $r_2$  value of the NSCs after internalization of CSeM/let-7b NPs led to high prominent  $T_2$  contrast even at low iron concentrations (Figure 3h). As

shown in Figure 3i, NSCs with CSeM/let-7b NPs had an  $r_2$  value of  $276.1 \text{ mM}^{-1} \text{ s}^{-1}$ , which was sufficiently high for in vivo MRI application after transplantation.

TLX (NR2E1), an orphan nuclear receptor highly expressed in the adult brain, is an essential intrinsic regulator that is involved in both maintaining the proliferation and inhibiting the differentiation of NSCs.<sup>31</sup> According to recent studies, decreased let-7b upregulated the expression of TLX, which led to reduced differentiation of NSCs.<sup>32</sup> After treatment with free let-7b antisense oligonucleotide and NPs, the TLX expression in NSCs was measured by Western blot (Figure 4a,b). Compared with the PBS group, the level of TLX expression was increased 2.5- and 2.1-fold in NSCs treated with the CSeM/let-7b and CH/M/let-7b NPs, respectively. The transfection efficiency of CSeM/let-7b NPs was comparable to that of Lipofectamine 2000. CSeM NPs with negative control antisense oligonucleotide showed no effect. These results meant that NPs with let-7b antisense oligonucleotide could significantly upregulate TLX expression due to their excellent cellular uptake and efficient endosomal/lysosomal escape.

Subsequently, the effect of NPs on exogenous NSC differentiation was characterized via immunolabeling with microtubule-associated protein 2 (MAP-2) to label neurons (green) and glial fibrillary acidic protein (GFAP) for glial cells (red). In the PBS control group, the majority of NSCs differentiated into glial cells and neurons (Figure 4c) with the mean fluorescence intensity of 7.19 (Figure 4d) and 8.44 (Figure 4e), respectively. The free let-7b antisense oligonucleotide had almost no reduction effect because of its poor cellular uptake. In the CSeM/let-7b and CH/M/let-7b NPs cultures, both MAP-2 and GFAP markers were significantly decreased due to their upregulated TLX expression. NSCs were shown previously to have a higher endogenous ROS level.<sup>33</sup> More NSCs had a higher level of ROS with the highest mean fluorescence intensity for the CSeM/let-7b and CH/M/let-7b NP groups (Figure S18), reaffirming their excellent effect on reducing NSC differentiation.

To further examine the BDNF level in NSCs cultures after treatment with NPs, we quantified BDNF level by sandwich ELISA. Compared with the PBS group, CSeM/let-7b NPs (170.8%) significantly increased the BDNF level in the culture medium (Figure 4f). With a comparable ability of decreasing NSC differentiation, the BDNF level for CSeM/let-7b NPs was much higher than that of CH/M/let-7b NPs (120.3%). This was attributed to their higher loading content of simvastatin. Additionally, NPs with negative control antisense oligonucleotide (108.7%), free let-7b antisense oligonucleotide (102.9%), and simvastatin (113.8%) had weak effect on the BDNF secretion due to the differentiation of NSCs. Therefore, the traceable CSeM/let-7b NPs with higher simvastatin loading content could efficiently control exogenous NSCs to produce BDNF.

The effect of BDNF on the proliferation of endogenous NSCs was investigated by immunostaining with the proliferation marker 5-bromo-2'-deoxyuridine (BrdU). NSCs cultured with the culture medium from exogenous NSCs for CSeM/let-7b NPs displayed more BrdU-positive cells (Figure 4g and Figure S19). These results suggested that an elevated level of BDNF after CSeM/let-7b NPs treatment could significantly induce the proliferation of NSCs.

Encouraged by the potency of CSeM/let-7b NPs in vitro, we next evaluated the therapeutic efficacy in vivo. Each APPsw/PS1dE9 double transgenic mouse (2xTg-AD) was stereotactically

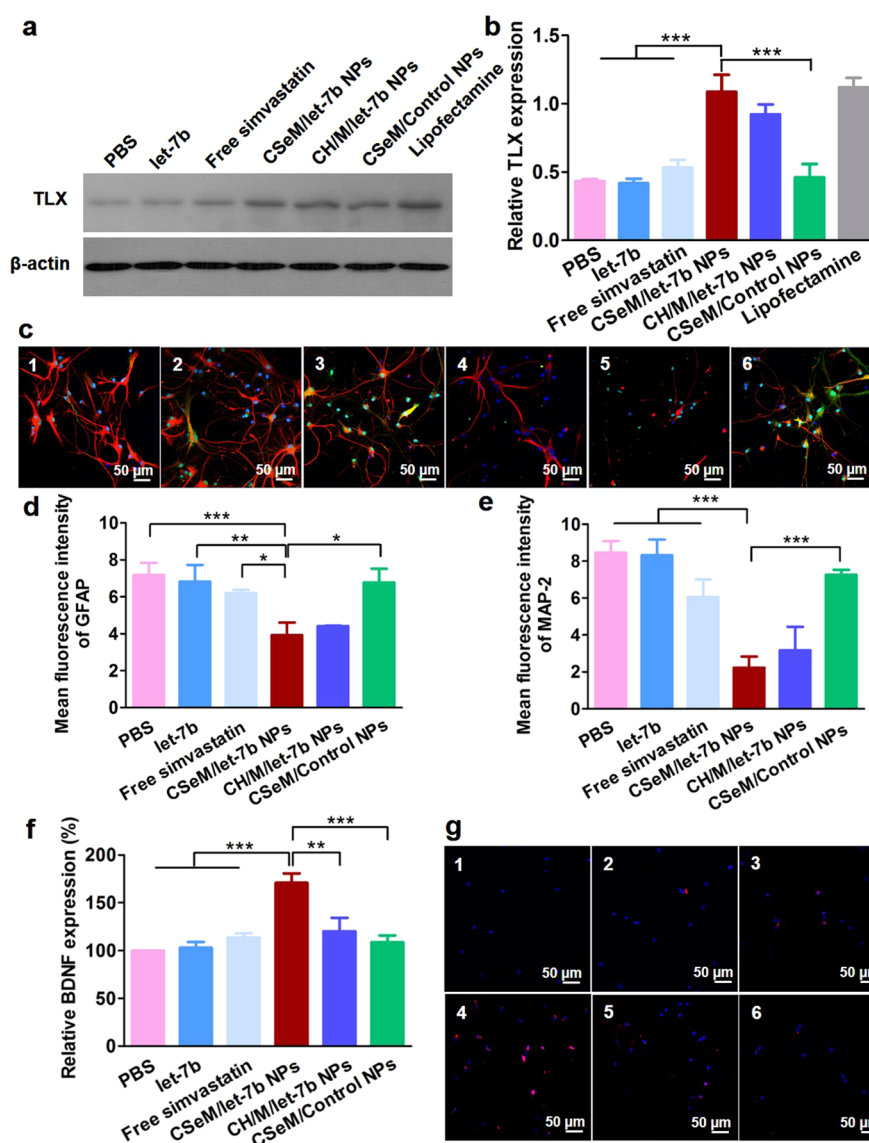


**Figure 4.** In vitro evaluation of the traceable NPs. (a) Western blot results of TLX expression after 48 h of incubation. Western bands were scanned and normalized to the internal control  $\beta$ -actin. (b) Quantified results of Western blot using ImageJ. (c) Neural differentiation of NSCs treated with NPs for 7 days. Cells were immunostained with MAP-2 (green) and GFAP (red). Quantified analysis of neural differentiation in panel c using software in CLSM: (d) mean fluorescence intensity of GFAP for glial cells; (e) mean fluorescence intensity of MAP-2 for neurons. (f) Relative BDNF expression detected in culture medium after 7 days treatment. (g) The proliferation of NSCs immunostained with BrdU (red) after culturing in primary culture medium for 7 days. The primary culture medium was obtained from exogenous NSCs after culturing with different samples for 7 days. Samples: (1) PBS, (2) let-7b antisense oligonucleotide, (3) free simvastatin, (4) CSeM/let-7b NPs, (5) CH/M/let-7b NPs, (6) CSeM/Control NPs. All nuclei in CLSM images were stained with DAPI. The mean  $\pm$  SD is shown ( $n = 3$ ). \* $P < 0.05$ , \*\* $P < 0.01$ , \*\*\* $P < 0.005$ .

cally injected at the right brain with  $5 \mu\text{L}$  of exogenous NSCs at a rate of  $1 \mu\text{L}/3 \text{ min}$ . Before transplantation, exogenous NSCs in 6-well plates were cultured with  $3 \mu\text{g}/\text{well}$  free let-7b antisense oligonucleotide or NPs for 4 h. Morris water maze (MWM) experiments were performed 30 days after treatment. As expected, mice treated with the produced CSeM/let-7b NP-NSCs displayed significantly shorter escape latencies (Figure 5a,b), indicating that exogenous NSCs treated with CSeM/let-7b NPs remarkably improved the cognition and memory of 2xTg-AD mice. These results were further confirmed by the fact that mice treated with CSeM/let-7b NP-NSCs crossed the platform location significantly more frequently than other groups (Figure 5c). To explore the effect of transplanted exogenous NSCs in detail, we next examined the BDNF level in the NSC-injected brain by Western blot and observed a

significant increment for the CSeM/let-7b NP-NSC-treated mice (Figure 5d and Figure S20).

We further assessed their influence on the proliferation of newly generated cells in the hippocampus. There were significantly more BrdU-positive cells in the CSeM/let-7b NP-NSC-treated mice than the amount of positive cells in the other mice, shown with arrows (Figures S21 and S22). With a comparable differentiation fate for CSeM/let-7b and CH/M/let-7b NP-treated exogenous NSCs, there were more nestin-positive NSCs in the CSeM/let-7b NP-NSC-treated mice than in the CH/M/let-7b NP-NSC-treated group (Figure S21a). These results indicated that the transplantation of exogenous NSCs treated with CSeM/let-7b NPs could effectively promote the proliferation of endogenous NSCs due to their secretion of more BDNF. Interestingly, the MAP-2 for neurons was

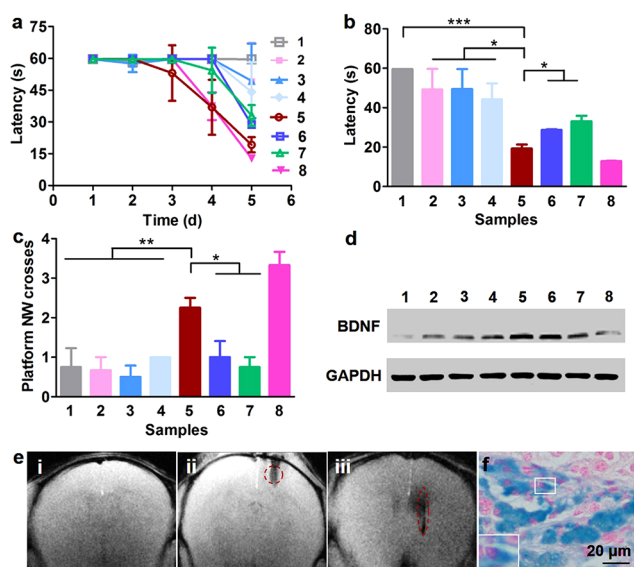


**Figure 5.** In vivo therapeutic efficiency. In MWM experiment, each trained 2xTg-AD mouse was allowed to swim freely for 60 s with the starting point far away from the platform. (a) Escape latency of 2xTg-AD mice during MWM at 1 to 5 days. (b) Escape latency of 2xTg-AD mice at 5 days. (c) Times that 2xTg-AD mice crossed the platform in the target quadrant. The mean  $\pm$  SD is shown ( $n = 5$ ). (d) Western blot results of BDNF expression in brain after 7 days of exogenous NSC transplantation. Western bands were scanned and normalized to the internal control glyceraldehyde-3-phosphate dehydrogenase (GAPDH). The mean  $\pm$  SD is shown ( $n = 3$ ). Samples: (1) saline, (2) NSCs alone, (3) let-7b antisense oligonucleotide-NSCs, (4) simvastatin-NSCs, (5) CSeM/let-7b NP-NSCs, (6) CH/M/let-7b NP-NSCs, (7) CSeM/Control NP-NSCs, (8) wild. In vivo MRI of the traceable CSeM/let-7b NPs.  $T_2^*$  MRI images of the 2xTg-AD were taken before and after 2 and 28 days of transplantation. MRI study was carried out at the 7 T MRI system. (e) Representative in vivo  $T_2^*$  MRI images of brain in 2xTg-AD mice, before transplantation (i) and 2 days (ii) and 28 days (iii) after transplantation. (f) Prussian blue staining in brain from panel e(iii). \* $P < 0.05$ , \*\* $P < 0.01$ , \*\*\* $P < 0.005$ .

significantly increased (Figure S21b) and GFAP immunoreactivity for glial cells was decreased (Figure S21c) in the CSeM/let-7b NP-NSC-treated mice. Therefore, the ameliorating neurologic changes resulted in better therapeutic efficacy of 2xTg-AD mice due to the synergistic effect on controlling exogenous NSCs as BDNF source for the traceable CSeM/let-7b NPs.

During the therapeutic process, the traceability of CSeM/let-7b NPs in vivo was observed using  $T_2^*$  MRI. Compared with the image before transplantation (Figure 5e(i)), the injection site was clearly detected in the ventricular system 2 days after transplantation (Figure 5e(ii)). A subsequent MRI was performed after 4 weeks and showed that NSCs extended posteriorly from the injection site into the hippocampus (Figure 5e(iii)), as also detected by Prussian blue staining (Figure 5f). As the magnified image shows, the SPIONs were around the nucleus in Prussian blue staining. Furthermore, eosin was used to stain the cytoplasm. The SPIONs were overlapped with cytoplasm eosin label (Figure S23). These results demonstrated that the SPIONs were still colocalized with the NSCs for long-term tracing in real time after transplantation. In general, our results demonstrated that CSeM/let-7b NPs allowed tracing of exogenous NSCs in real time and synergistically improved the learning and memory of 2xTg-AD mice.

## CONCLUSION

In summary, we have developed a kind of traceable NP self-assembled from the positively charged polyprodrug amphiphiles with enhanced drug loading and ROS-responsive release ability, which could effectively control exogenous NSCs as BDNF source for traceable synergistic therapy of AD. CSeM/let-7b NPs significantly elevated the secretion of BDNF for exogenous NSCs and promoted the proliferation and neurogenesis of endogenous NSCs. The treatment resulted in better rescuing the memory deficits in 2xTg-AD mice. Moreover, the system traced the transplantation site and migration of exogenous NSCs via MRI because of the high  $r_2$  value of SPIONs. Therefore, the traceable NPs might have the potential to open up a new avenue for treatment application for AD as well as other neurodegenerative disorders because of the good tracing and therapeutic ability.

## ASSOCIATED CONTENT

### Supporting Information

The Supporting Information is available free of charge on the ACS Publications website at DOI: 10.1021/jacs.8b01641.

Experimental details, characterization methods, and all relevant characterization data (PDF)

## AUTHOR INFORMATION

### Corresponding Author

\*xzhang@ipe.ac.cn

### Author Contributions

All authors have given approval to the final version of the manuscript.

### Notes

The authors declare no competing financial interest.

## ACKNOWLEDGMENTS

This work was financially supported by the National High Technology Research and Development Program (2016YFA0200303), the National Natural Science Foundation of China (31522023, 51373177, 51573188), the Beijing Natural Science Foundation (L172046), the Beijing Municipal Science & Technology Commission (Z161100002616015), and the "Strategic Priority Research Program" of the Chinese Academy of Sciences (XDA09030301-3).

## REFERENCES

- (a) Ehrnhoefer, D. E.; Wong, B. K. Y.; Hayden, M. R. *Nat. Rev. Drug Discovery* **2011**, *10*, 853–867. (b) Rodriguez-Rodríguez, C.; Sánchez de Groot, N.; Rimola, A.; Álvarez-Larena, Á.; Lloveras, V.; Vidal-Gancedo, J.; Ventura, S.; Vendrell, J.; Sodupe, M.; González-Duarte, P. *J. Am. Chem. Soc.* **2009**, *131*, 1436–1451.
- (a) Munoz, J. R.; Stoutenger, B. R.; Robinson, A. P.; Spees, J. L.; Prockop, D. J. *Proc. Natl. Acad. Sci. U. S. A.* **2005**, *102*, 18171–18176. (b) Arvidsson, A.; Collin, T.; Kirik, D.; Kokaia, Z.; Lindvall, O. *Nat. Med.* **2002**, *8*, 963–970.
- (a) Tan, J.; Wang, Y.; Yip, X.; Glynn, F.; Shepherd, R. K.; Caruso, F. *Adv. Mater.* **2012**, *24*, 3362–3366. (b) Islam, O.; Loo, T. X.; Heese, K. *Curr. Neurovasc. Res.* **2009**, *6*, 42–53.
- Blurton-Jones, M.; Kitazawa, M.; Martinez-Coria, H.; Castello, N. A.; Müller, F. J.; Loring, J. F.; Yamasaki, T. R.; Poon, W. W.; Green, K. N.; LaFerla, F. M. *Proc. Natl. Acad. Sci. U. S. A.* **2009**, *106*, 13594–13599.
- (a) Imitola, J.; Raddassi, K.; Park, K. I.; Mueller, F. J.; Nieto, M.; Teng, Y. D.; Frenkel, D.; Li, J.; Sidman, R. L.; Walsh, C. A.; Snyder, E. Y.; Khoury, S. J. *Proc. Natl. Acad. Sci. U. S. A.* **2004**, *101*, 18117–

18122. (b) Müller, F. J.; Snyder, E. Y.; Loring, J. F. *Nat. Rev. Neurosci.* **2006**, *7*, 75.
- (6) (a) Kirby, E. D.; Kuwahara, A. A.; Messer, R. L.; Wyss-Coray, T. *Proc. Natl. Acad. Sci. U. S. A.* **2015**, *112*, 4128–4133. (b) Kamei, N.; Tanaka, N.; Oishi, Y.; Hamasaki, T.; Nakanishi, K.; Sakai, N.; Ochi, M. *Spine* **2007**, *32*, 1272. (c) Pluchino, S.; Quattrini, A.; Brambilla, E.; Gritti, A.; Salani, G.; Dina, G.; Galli, R.; Del Carro, U.; Amadio, S.; Bergami, A.; Furlan, R.; Comi, G.; Vescovi, A. L.; Martino, G. *Nature* **2003**, *422*, 688.
- (7) Guzman, R.; Uchida, N.; Bliss, T. M.; He, D.; Christopherson, K. K.; Stellwagen, D.; Capela, A.; Greve, J.; Malenka, R. C.; Moseley, M. E.; Palmer, T. D.; Steinberg, G. K. *Proc. Natl. Acad. Sci. U. S. A.* **2007**, *104*, 10211–10216.
- (8) (a) Ni, N.; Zhang, D.; Xie, Q.; Chen, J.; Wang, Z.; Deng, Y.; Wen, X.; Zhu, M.; Ji, J.; Fan, X.; Luo, M.; Gu, P. *Sci. Rep.* **2015**, *4*, 6671. (b) Zhao, C. N.; Sun, G.; Li, S.; Lang, M. F.; Yang, S.; Li, W.; Shi, Y. *Proc. Natl. Acad. Sci. U. S. A.* **2010**, *107*, 1876–1881.
- (9) (a) Wu, H. T.; Lu, D. Y.; Jiang, H.; Xiong, Y.; Qu, C. S.; Li, B.; Mahmood, A.; Zhou, D.; Chopp, M. J. *Neurotraum.* **2008**, *25*, 130–139. (b) Han, X. G.; Yang, N.; Xu, Y. S.; Zhu, J. L.; Chen, Z. Q.; Liu, Z. J.; Dang, G. T.; Song, C. L. *Neurosci. Lett.* **2011**, *487*, 255–259.
- (10) (a) Park, J. S.; Park, W.; Park, S. J.; Larson, A. C.; Kim, D. H.; Park, K. H. *Adv. Funct. Mater.* **2017**, *27*, 1700396. (b) Hu, B. B.; Zeng, M.; Chen, J. L.; Zhang, Z. Z.; Zhang, X. N.; Fan, Z. M.; Zhang, X. *Small* **2016**, *12*, 4707–4712.
- (11) (a) Dinauer, N.; Lochmann, D.; Demirhan, I.; Bouazzaoui, A.; Zimmer, A.; Chandra, A.; Kreuter, J.; Von Briesen, H. *J. Controlled Release* **2004**, *96*, 497–507. (b) Barreto, J. A.; O'Malley, W.; Kubeil, M.; Graham, B.; Stephan, H.; Spiccia, L. *Adv. Mater.* **2011**, *23*, H18–H40.
- (12) Wang, K.; Hu, Q. D.; Zhu, W.; Zhao, M. M.; Ping, Y.; Tang, G. P. *Adv. Funct. Mater.* **2015**, *25*, 3380.
- (13) Gaspar, V. M.; Gonçalves, C.; De Melo-Diogo, D.; Costa, E. C.; Queiroz, J. A.; Pichon, C.; Sousa, F.; Correia, I. J. *J. Controlled Release* **2014**, *189*, 90–104.
- (14) Shen, Y. Q.; Jin, E. L.; Zhang, B.; Murphy, C. J.; Sui, M. H.; Zhao, J.; Wang, J. Q.; Tang, J. B.; Fan, M. H.; Van Kirk, E.; Murdoch, W. J. *J. Am. Chem. Soc.* **2010**, *132*, 4259–4265.
- (15) Blass, J. P. *J. Neurosci. Res.* **2001**, *66*, 851–856.
- (16) Cheng, Y. L.; Yumul, R. C.; Pun, S. H. *Angew. Chem., Int. Ed.* **2016**, *55*, 12013–12196.
- (17) Lok, C. N.; Zou, T. T.; Zhang, J. J.; Lin, I. W. S.; Che, C. M. *Adv. Mater.* **2014**, *26*, 5550–5557.
- (18) (a) Li, Y.; Cheng, Q.; Jiang, Q.; Huang, Y. Y.; Liu, H. M.; Zhao, Y. L.; Cao, W. P.; Ma, G. H.; Dai, F. Y.; Liang, X. J.; Liang, Z. C.; Zhang, X. *J. Controlled Release* **2014**, *176*, 104–114. (b) Zhang, R.; Li, Y.; Hu, B. B.; Lu, Z. G.; Zhang, J. C.; Zhang, X. *Adv. Mater.* **2016**, *28*, 6345–6352. (c) Li, Y.; Liu, R. Y.; Yang, J.; Ma, G. H.; Zhang, Z. Z.; Zhang, X. *Biomaterials* **2014**, *35*, 9731–9745.
- (19) (a) Le Belle, J. E.; Orozco, N. M.; Paucar, A. A.; Saxe, J. P.; Mottahedeh, J.; Pyle, A. D.; Wu, H.; Kornblum, H. I. *Cell Stem Cell* **2011**, *8*, 59–71. (b) Tapeinos, C.; Pandit, A. *Adv. Mater.* **2016**, *28*, 5553–5585.
- (20) (a) Hu, X. L.; Hu, J. M.; Tian, J.; Ge, Z. S.; Zhang, G. Y.; Luo, K. F.; Liu, S. Y. *J. Am. Chem. Soc.* **2013**, *135*, 17617–17629. (b) Hu, X. L.; Liu, G. H.; Li, Y.; Wang, X. R.; Liu, S. Y. *J. Am. Chem. Soc.* **2015**, *137*, 362–368.
- (21) Ren, H. F.; Wu, Y. T.; Ma, N.; Xu, H. P.; Zhang, X. *Soft Matter* **2012**, *8*, 1460–1466.
- (22) (a) Tao, Y. F.; He, J. L.; Zhang, M. Z.; Hao, Y.; Liu, J.; Ni, P. H. *Polym. Chem.* **2014**, *5*, 3443–3452. (b) Li, L. Y.; Raghupathi, K.; Song, C. F.; Prasad, P.; Thayumanavan, S. *Chem. Commun.* **2014**, *50*, 13417–13432. (c) Chi, X. D.; Ji, X. F.; Xia, D. Y.; Huang, F. H. *J. Am. Chem. Soc.* **2015**, *137*, 1440–1443.
- (23) Awino, J. K.; Gudipati, S.; Hartmann, A. K.; Santiana, J. J.; Cairns-Gibson, D. F.; Gomez, N.; Rouge, J. L. *J. Am. Chem. Soc.* **2017**, *139*, 6278–6281.
- (24) (a) Zhang, Z. Y.; Xu, Y. D.; Ma, Y. Y.; Qiu, L. L.; Wang, Y.; Kong, J. L.; Xiong, H.-M. *Angew. Chem., Int. Ed.* **2013**, *52*, 4127–4131.
- (b) Chen, R. J.; Khormaei, S.; Eccleston, M. E.; Slater, N. K. H. *Biomacromolecules* **2009**, *10*, 2601–2608.
- (25) Ma, N.; Li, Y.; Xu, H. P.; Wang, Z. Q.; Zhang, X. *J. Am. Chem. Soc.* **2010**, *132*, 442–443.
- (26) Park, D.; Xiang, A. P.; Mao, F. F.; Zhang, L.; Di, C. G.; Liu, X. M.; Shao, Y.; Ma, B. F.; Lee, J. H.; Ha, K. S.; Walton, N.; Lahn, B. T. *Stem Cells* **2010**, *28*, 2162–2171.
- (27) Yoneyama, M.; Kawada, K.; Gotoh, Y.; Shiba, T.; Ogita, K. *Neurochem. Int.* **2010**, *56*, 740–746.
- (28) Li, Y.; Liu, R. Y.; Shi, Y. J.; Zhang, Z. Z.; Zhang, X. *Theranostics* **2015**, *5*, 583.
- (29) Dean, N. M.; Bennett, C. F. *Oncogene* **2003**, *22*, 9087–9096.
- (30) (a) Yu, T. Z.; Liu, X. X.; Bolcato-Bellemin, A.; Wang, Y.; Liu, C.; Erbacher, P.; Qu, F. Q.; Rocchi, P.; Behr, J. P.; Peng, L. *Angew. Chem.* **2012**, *124*, 8606–8612. (b) Benjaminsen, R. V.; Matthebjerg, M. A.; Henriksen, J. R.; Moghimi, S. M.; Andresen, T. L. *Mol. Ther.* **2013**, *21*, 149–157.
- (31) (a) Zhao, C. N.; Sun, G. Q.; Ye, P.; Li, S. X.; Shi, Y. H. *Sci. Rep.* **2013**, *3*, 1329. (b) Shi, Y. H.; Chichung Lie, D.; Taupin, P.; Nakashima, K.; Ray, J.; Yu, R. T.; Gage, F. H.; Evans, R. M. *Nature* **2004**, *427*, 78. (c) Qu, Q. H.; Sun, G. Q.; Li, W. W.; Yang, S.; Ye, P.; Zhao, C. N.; Yu, R. T.; Gage, F. H.; Evans, R. M.; Shi, Y. H. *Nat. Cell Biol.* **2010**, *12*, 31.
- (32) Murai, K.; Sun, G. Q.; Ye, P.; Tian, E.; Yang, S.; Cui, Q.; Sun, G. H.; Trinh, D.; Sun, O.; Hong, T.; Wen, Z. X.; Kalkum, M.; Riggs, A. D.; Song, H. J.; Ming, G. L.; Shi, Y. H. *Nat. Commun.* **2016**, *7*, 10965.
- (33) Kobayashi, C. I.; Suda, T. *J. Cell. Physiol.* **2012**, *227*, 421–430.